Tracking of Autologous VSOP-Labeled Mesenchymal Stem Cells in the Sheep Brain Using 3.0 T MRI

8

Antje Y. Dreyer, Donald Lobsien, Claudia Pösel, Karl-Titus Hoffmann, Björn Nitzsche, Matthias Findeisen, Albrecht Stroh, and Johannes Boltze

8.1 Introduction

Ischemic stroke is among the pathological conditions with highest mortality and morbidity in Western societies (Langhorne et al. 2011). Despite significant improvements of clinical treatment regimen, particularly the introduction of the stroke unit concept, the disease is still one of the major causes of death and the most important reason for permanent disability in adulthood (Bonita et al. 2004).

A.Y. Dreyer • J. Boltze (✉)
Department of Cell Therapy, Fraunhofer-Institute for Cell Therapy and Immunology, Perlickstraße 1, D-04103 Leipzig, Germany

Translational Centre for Regenerative Medicine, University of Leipzig, Philipp-Rosenthal-Straße 55, D-04103 Leipzig, Germany
e-mail: antje.dreyer@izi.fraunhofer.de; johannes.boltze@izi.fraunhofer.de

D. Lobsien • K.-T. Hoffmann
Department for Neuroradiology, University of Leipzig, Liebigstraße 20, D-04103 Leipzig, Germany
e-mail: donald.lobsien@medizin.uni-leipzig.de; karl-titus.hoffmann@medizin.uni-leipzig.de

C. Pösel • B. Nitzsche
Department of Cell Therapy, Fraunhofer-Institute for Cell Therapy and Immunology, Perlickstraße 1, D-04103 Leipzig, Germany
e-mail: claudia.poesel@izi.fraunhofer.de; bjoern.nitzsche@izi.fraunhofer.de

M. Findeisen
Department of Chemistry and Mineralogy, Institute of Analytical Chemistry, University of Leipzig, Johannisallee 29, D-04103 Leipzig, Germany
e-mail: findeis@rz.uni-leipzig.de

A. Stroh
Focus Group Translational Neurosciences (FTN), Institute for Microscopic Anatomy and Neurobiology, Johannes Gutenberg-University Mainz, Hanns-Dieter-Hüsch-Weg 19, D-55128 Mainz, Germany
e-mail: albrecht.stroh@unimedizin-mainz.de

J. Jolkkonen, P. Walczak (eds.), *Cell-Based Therapies in Stroke*,
DOI 10.1007/978-3-7091-1175-8_8, © Springer-Verlag Wien 2013

Treatment interventions mainly focus on the recanalization of the occluded vessel with alteplase (recombinant tissue plasminogen activator, tPA) as the sole effective and FDA-approved therapeutic approach (Falluji et al. 2012). Next to the thrombolytic approach, the use of anticoagulative/antiplatelet drugs for the prevention of secondary ischemic events (Emre et al. 2007) and decompressive hemicraniectomy as a symptomatic therapy in case of malignant middle cerebral artery (MCA) occlusion (Vahedi et al. 2007) are implemented in clinical stroke management guidelines. Even though the therapeutic time window for thrombolysis by tPA was recently extended from 3.0 to 4.5 h upon stroke onset (Lansberg et al. 2009), numerous contraindications as well as an increasing risk for hemorrhagic transformation at later time points (Shobha et al. 2011) still exclude most patients from treatment. Interventional approaches aiming at clot removal or local thrombolysis can be safe and effective within a time window of up to 8.0 h (Natarajan et al. 2009) but require an experienced team of interventional radiologists and are restricted to a few, highly specialized centers.

Hence, there is a strong demand for alternative therapeutic approaches with stem cell and cell-based therapies currently being among the most promising options (Burns and Steinberg 2011). Evidence for neuronal differentiation and/or beneficial effects after transplantation were shown for a multitude of stem and progenitor cell populations in experimental studies using animal models of focal cerebral ischemia. These comprehensive investigations revealed the therapeutic potential of embryonic stem cells (Nagai et al. 2010), neural progenitor cells (Minnerup et al. 2011), and induced pluripotent stem cells (Jensen et al. 2011). However, those cell populations are either available from non-autologous sources only or bear the risk of malignant transformation after transplantation (Seminatore et al. 2010). This currently limits the applicability of the cells in a clinical setup. Autologous sources of adult stem cells may represent a reasonable alternative. Bone marrow-derived stromal cells (BMSC), a kind of mesenchymal stem cells (MSC), were reported to reduce functional deficits (Shen et al. 2007b) and ischemic lesion size (Ukai et al. 2007) and do not show signs of malignant transformation and excessive tissue overgrowth after transplantation. Notably, these cells may enhance angiogenesis and neurogenesis following stroke (Bao et al. 2011) and are further supposed to modulate reactive gliosis in a pro-regenerative manner (Shen et al. 2008). Therapeutic effects were also reported for MSC from other sources including adipose tissue (Kranz et al. 2010) and umbilical cord matrix (Lin et al. 2011), corroborating the anticipated therapeutic potential of MSC. Consequently, the safety of cell-based therapies using autologous bone marrow-derived MSC was already assessed in early-stage clinical trials (Bang et al. 2005; Honmou et al. 2011). However, relevant modes of action as well as the optimal transplantation route still need to be elucidated. Detailed knowledge about the biodistribution of cells after local or systemic administration will complement our understanding of the therapeutic mechanisms and is considered important for assessing safety aspects, which is also essential from a regulatory perspective.

8.1.1 Approaches for Stem Cell Labeling and Tracking in Large Animal Models

Different labeling techniques are applied to track administered cells in vivo. Bioluminescence imaging (BLI) gives relevant spatial and semiquantitative information on cell distribution and homing (Jang et al. 2010) but is restricted to smaller organisms due to the limited light penetration through biological tissue. Single photon emission computed tomography (SPECT) uses gamma-emitting marker radioisotopes and allows reliable signal quantification in experimental animals and human patients but provides poor spatial resolution and anatomical information. SPECT was already applied to detect technetium-99 m-labeled bone marrow-derived cells in patients after intra-arterial delivery (Barbosa da Fonseca et al. 2010), even though repeated investigations have to be considered with care to minimize the radioactive burden. Magnetic resonance imaging (MRI) was shown to be feasible for cell tracking in both, experimental subjects (Muja and Bulte 2009) and human patients (de Vries et al. 2005), and MRI scans can be performed repeatedly and without relevant risks, enabling time course studies. Moreover, excellent spatial and anatomical information can be obtained due to the submillimeter resolution of this imaging modality. In experimental setups, T2- and T2*-weighted imaging sequences are best suitable for tracking locally (Kim et al. 2008; Daadi et al. 2009) or systemically (Stroh et al. 2006) administered cells in rodent models of stroke after paramagnetic cell labeling. Small bore 7.0 T, 9.4 T, or even 17.6 T dedicated animal scanners were used for this purpose. Application of those high field strengths and tailored scanning sequences allows for isotropic resolutions of less than 100 μm, with excellent sensitivity toward labeled cells, detecting 100 or less cells in the brain (Stroh et al. 2005). However, the use of high field strength (7.0 T or more) human scanners is mainly restricted to experimental studies at the moment. These scanners will not be available in most centers in the foreseeable future.

International expert committees recommend the validation of cell-based therapeutic strategies for stroke in large animal models before translating experimental approaches into clinical trials. Better anatomical discrimination between gray and white matter in the gyrencephalic brain as well as the assessment of specific cell delivery options in large animal models are considered advantageous (Savitz et al. 2011). Moreover, autologous cell therapies may be performed more easily as compared to small animal species. The use of large animal models is also relevant from an imaging perspective, since the investigation of both human patients and large animals necessitates the use of clinical MRI scanners with lower field strengths (commonly 3.0 T), wider bores, and different resonance coil sets. Larger bore diameters result in magnetic field inhomogeneities which have to be compensated and taken into consideration when translating experimental imaging sequences to clinical scanners. These aspects can be investigated best by using a combination of large animal models and clinical scanners. The ovine brain has been reported feasible for advanced imaging studies using clinical scanners, and a model of focal cerebral ischemia is available in the species (Boltze et al. 2008).

A comprehensive set of experimental studies was designed to reveal the optimal labeling protocol as well as the in vitro detection limits for ovine MSC in using T2* sequences at 3.0 T. The in vivo detection limit for autologous ovine MSC and their discrimination from hemorrhagic events in the sheep brain were assessed after local cell administration using the same magnetic field strength, while methods for the histological identification of transplanted cells have also been investigated. Finally, pilot experiments for cell tracking after intravenous MSC delivery in an ovine stroke model have been performed. The most notable results and consequences for translational approaches will be discussed in this chapter.

8.2 MRI of VSOP-Labeled Cells In Vitro

Bone marrow cell samples were harvested and processed as described elsewhere (Dreyer et al. 2012) from anesthetized healthy adult Merino sheep. Ovine MSC were separated from MNC according to a widely used separation method (Pittenger 2008). Very small superparamagnetic iron oxide particles (VSOP) were used for MSC labeling. It has been previously reported that incorporation of VSOP into cells causes a significant signal loss in T2*-weighted sequences (Arbab et al. 2003). Cytotoxic effects of VSOP labeling in lower concentrations (up to 3.0 mM) have not been observed in spleen- (Stroh et al. 2006) and bone marrow-derived MNC, as well as human cord blood MNC (Stroh et al. 2009). Only transient oxidative stress was reported to be induced in rodent macrophages at 3.0 mM (Stroh et al. 2004). The development of tailored labeling protocols is recommended to assess potential detrimental effects of labeling on the particular cell population used (Stroh et al. 2009). Thus, the previously reported VSOP labeling protocols were transferred to and optimized for ovine MSC, primarily by assessing the effect of different VSOP labeling molarities.

The transverse relaxation times of 9×10^5 cells in 3 mL PBS, either labeled with 1.5 or 3.0 mM VSOP, were measured at 0.47 T/20 MHz using a Bruker Minispec relaxometer and compared to relaxation time of unlabeled cells (Fig. 8.1a). There was a significant shortening of the relaxation time from 1,888 ± 171 ms (100 %) to 583 ± 190 ms (31 ± 11 %) for 1.5 mM ($p < 0.001$) and 434 ± 146 ms (23 ± 8 %) for 3.0 mM ($p < 0.001$). Moreover, incubation with 3.0 mM VSOP significantly reduced relaxation time as compared to 1.5 mM incubation concentration ($p < 0.05$).

Next, the impact of VSOP cell labeling on MSC viability was assessed. Cell numbers were counted using the trypan blue exclusion method (Fig. 8.1b) after the different labeling conditions. As compared to controls (100 %), there was a drop in the number of vital cells to 90 ± 19 % for 1.5 mM ($p > 0.05$) and 86 ± 16 % for 3.0 mM ($p < 0.05$) immediately after labeling. Viability rates remained almost constant until 4 h after VSOP incubation (91 ± 18 % for 1.5 mM and 89 ± 14 % for 3.0 mM). Additional MTT testing did not reveal signs of relatively reduced or enhanced metabolic activity between control conditions (set at 1.0) and cell samples immediately after labeling (1.5 mM: 1.10 ± 0.09; 3.0 mM: 0.98 ± 0.14;

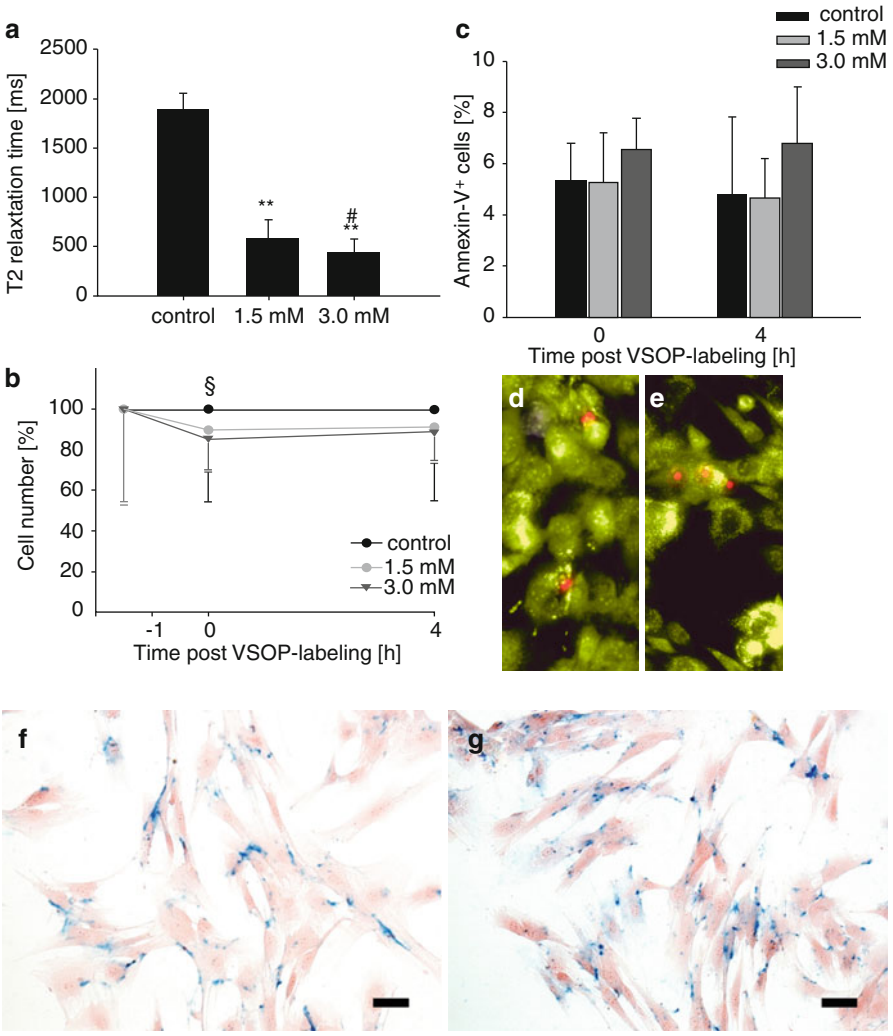

Fig. 8.1 VSOP-labeling of ovine MSC. Incubation of MSC with VSOP led to a significant reduction of T2 relaxation time (**a**, $p<0.001$). Increasing VSOP concentration from 1.5 to 3.0 mM further significantly shortened T2 relaxation time (**a**, $p<0.05$). Cell labeling slightly reduced viable cell numbers. This difference was statistically significant only immediately after labeling with 3.0 mM (**b**). Apoptosis rates, measured by annexin-V-staining, were not significantly affected by VSOP incubation at both molarities (**c**). This finding is in accordance with results from a life/dead-cell assay using acridine-orange (vital cells, *green*) and ethidium-bromide (dead cells, *orange-red*; **d**, **e**). Prussian-Blue-staining clearly showed intracellular iron deposits after labeling with 1.5 mM (**f**) and 3.0 mM (**g**). $^{**}p<0.001$ (versus control); #/§$p<0.05$ (versus 1.5 mM/3.0 mM). Scale bars: 50 µm

$p=0.154$) and 4 h later (1.5 mM: 0.90 ± 0.10; 3.0 mM: 1.00 ± 0.10; $p=0.940$). Moreover, apoptosis rates, being measured by cytometry-based detection of annexin V staining in MSC, were comparable to control conditions 4 h after

labeling (Fig. 8.1c) with apoptosis rates being 4.79 ± 3.04 % in control MSC populations versus 4.55 ± 1.57 % (1.5 mM) and 6.80 ± 2.20 % (3.0 mM) in labeled MSC, respectively ($p > 0.05$). Similar results were obtained using a live/dead assessment by acridine-orange (vital cells, green)/ethidium-bromide (dead cells, orange-red) staining (1.5 mM: Fig. 8.1d; 3.0 mM: Fig. 8.1e). Thus, it may be concluded that there is a loss of viable cells during VSOP labeling, especially after labeling with 3.0 mM VSOP. However, this cell loss is comparatively small and only occurs directly after labeling. Differences between 1.5 and 3.0 mM incubation molarities in other viability assays, even though not statistically significant, underline the necessity of additional long-term investigations. A follow-up of at least 24 h following labeling is required to detect a possible late detrimental effect of VSOP labeling on ovine MSC at 3.0 mM higher incubation molarities and to predict possible consequences for further research. Exemplary samples of labeled MSC after Prussian blue (PB) staining are given in Fig. 8.1f (1.5 mM) and Fig. 8.1g (3.0 mM). Since labeling with 3.0 mM VSOP gave superior result regarding relaxation time shortening, this concentration was chosen for MSC labeling in all further experiments.

In order to prepare experiments for MRI-based tracking of autologous MSC in vivo, the detection limit of the cells was assessed in gel phantoms. Those gel phantoms – in contrast to conventional small-scale test tube samples – can closely resemble cell distributions observed upon local in vivo administration or after homing of systemically administered cells to a particular site. Gel phantoms mimic both the magnetic properties of brain parenchyma and the diffusion constants. Thus, gel phantoms with injected cells may serve as ideal model for tailoring imaging sequences (Stroh et al. 2005) and are commonly used to investigate detection limits of labeled cells.

Since a potential homing of VSOP-labeled cells to an ischemic lesion in the brain can be supposed to result in areal signal extinctions in zones bordering the central infarct after systemic administration (Stroh et al. 2006; Tsai et al. 2011), agarose gel phantoms were used to simulate this effect with MSC being embedded in thin layers within the phantoms. Phantom one contained 0 unlabeled and 100, 500, and 5,000 labeled MSC, respectively, while phantom two contained 100,000 unlabeled and 1,000; 10,000; and 100,000 labeled cells (Fig. 8.2a).

Gel phantoms were placed in a Siemens Trio 3.0 T clinical MRI scanner equipped with an 8-channel coil. This coil is suitable for examinations of both humans and large animals and was therefore used in the experiments. A T2*-weighted sequence was conducted according to Table 8.1. Detection limits were assessed by three researchers with experience in radiological assessments but blinded to the experimental conditions. These researchers had to decide whether or not signal losses, presumably evoked by VSOP-labeled cells, are visible in a certain layer. Only in case all three investigators independently decided that this was the case, a cell number was declared detectable under the particular condition.

In the T2* sequence, gel phantoms were visualized as bright, homogenous structures with very rare signs for embedded air bubbles. No hypointensities based on signal losses were observed in layers containing no cells (Fig. 8.2b) or 100,000

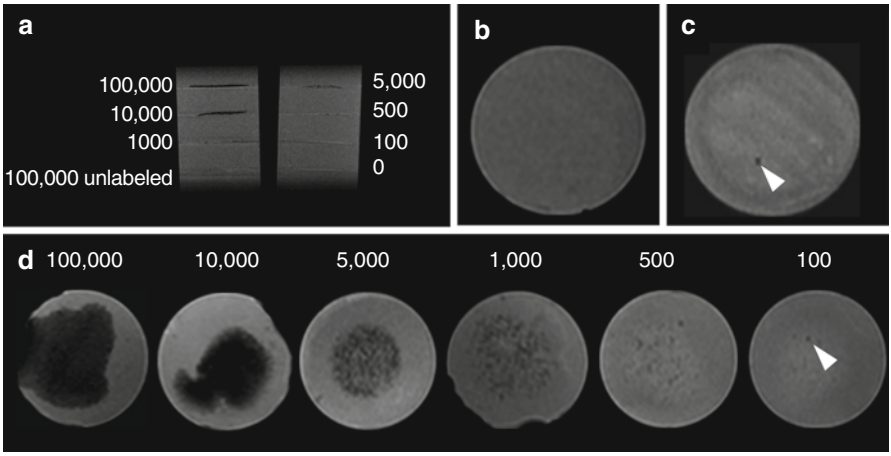

Fig. 8.2 Detection limit of VSOP-labeled MSC in gel phantoms at 3.0 T. Agarose gel phantoms containing horizontal layers of 0–100,000 labeled MSC or 100,000 unlabeled MSC were manufactured and measured at 3.0 T by applying a T2* sequence (see Table 8.1) (**a**). Cell-free gel layers (**b**) and 100,000 unlabeled MSC (**c**). Air bubbles inside the gel layers were rarely observed, causing small, punctual signal extinctions (**c**, *white arrow head*). Planar signal voids were observed in layers containing 1,000 or more cells, whereas 500 cells caused punctual signal losses within the layer (**d**). 100 cells (**d**, *white arrow head*) were not unambiguously discriminable from scattered air bubbles (**c**), thus the detection limit was found at 500 cells at 3.0 T in this experiment

Table 8.1 Design of T2* MR sequences for in vitro and in vivo investigations

	Sequence	Coil	TR/TE	Flip angle (°)	Bandwidth (Hz)	Averages	Voxel size (mm)	Scan time (min)
In vitro	T2* FLASH 3D	8 channel coil	620/20	20	200	1	0.55×0.47×0.6	314
In vivo	T2* FLASH 3D	4 channel flex coil	620/20	20	200	1	0.83×0.66×0.5	127

unlabeled MSC (Fig. 8.2c, note small air bubble, white arrow head) in horizontal slices. In contrast, 100,000 labeled cells became clearly visible (Fig. 8.2d) as planar signal losses which were clearly discriminable from the gel. Similar results were observed for 10,000; 5,000; and 1,000 cells with declining sizes of the planar signal losses (Fig. 8.2d). Five hundred labeled MSC per layer (Fig. 8.2d) could also be detected, but signal losses appeared as small punctae and not as planar signal extinctions. 100 cells per layer were not unambiguously detectable as distinction between the punctual signal extinction and rarely occurring single air bubbles was not possible (Fig. 8.2d, white arrow head). Thus, the detection limit was defined to range at 500 cells at 3.0 T, superior to 1.5 T (5,000 cells, data not shown).

8.3 MRI of VSOP-Labeled Cells In Vivo

In the next step the detection limit of VSOP-labeled cells in the ovine brain was investigated. This is of particular importance since the presence of blood vessels or hemorrhages in the brain can lead to false-positive results. Hemorrhages can be of traumatic origin (damage to small intracerebral vessels during local cell injections) or may occur consecutively after major territorial ischemia.

However, scans of defined duration (more than 5 h) can only be performed with difficulties in sheep, since prolonged anesthesia (>4 to 8 h) may have detrimental metabolic effects and can cause hypothermia with compensatory shivering, which severely affects image quality. Very long anesthesia (8 h or more) will result in poor recovery rates in sheep (Boltze et al. 2008). Considering animal transfer to and from the scanner as well as setup and planning sequences, scanning times in sheep are not recommended to exceed 4 h to ensure maximum image quality and animal welfare. Therefore, tailoring of imaging sequences resulting in shortening of scan time became necessary for in vivo experiments (see Table 8.1), unavoidably resulting in a compromise between image quality and sequence usability.

A two-step approach was chosen to consider this situation. First, the detection limit for VSOP-labeled MSC was assessed in the healthy sheep brain after stereotaxic injection of a defined cell number. In the second step, potential cell homing to the ischemic brain after intravenous MSC injection was investigated.

Frameless stereotaxic transplantations were planned and conducted using the Brainsight™ stereonavigation system as previously described in detail (Frey et al. 2004). The system was slightly modified by the supplier to fit special anatomical characteristics of the ovine skull. Six sheep were used in this experiment. A three-dimensional T1 MR dataset of the brain (minimum resolution $1 \times 1 \times 1$ mm) including fiducial markers and a time-of-flight MR angiography (to detect major vessels) were obtained 1 day before surgery. The fiducial markers were fixed to a maxillary splint which is adaptable to the individual shapes of the maxillary molars and the hard palate, allowing a precise and reproducible positioning for each investigated animal. MR imaging was completed within an hour. Two trajectories for stereotaxic cell administration, one in each hemisphere, were planned avoiding close spatial proximity to blood vessels (exception: animal 1, see below). The white matter of the corona radiata was the preferred target location due to its relatively homogenous MRI signal. Predefined numbers of VSOP-labeled cells were injected according to Table 8.2. Labeling was done using 3.0 mM VSOP, and labeling efficacy was confirmed by relaxometry as described above (Sect. 8.2).

The stereotaxic implementation of the cells was performed without complications in all subjects, and maximum deviation between planned and realized trajectory was 1.0 mm in each dimension. In animal 1, serving as a control subject, 50 μL PBS not containing VSOP-labeled MSC was injected into the left hemisphere, and a hemorrhage was induced contralaterally by targeted damage of a small arterial blood vessel.

Locally transplanted animals were subjected to one MRI investigation using a T2* sequence which had been designed as a compromise of image quality and

Table 8.2 Cell deposits in sheep receiving local stereotaxic cell transplantation

Subject no.	1	2	3	4	5	6
Left hemisphere	PBS	100,000	100,000	10,000	10,000	10,000
Right hemisphere	Hemorrhage induced	1,000	1,000	500	500	500

examination time (for imaging parameters refer to Table 8.1). Imaging series were analyzed by three blinded investigators in accordance to the gel phantom assessment.

Injection of PBS did not result in any detectable signal extinction (Fig. 8.3a), whereas induction of moderate hemorrhage resulted in a clear signal loss (about 54 × 23 mm) (Fig. 8.3b). 100,000 VSOP-labeled MSC appeared as an ellipsoid hypointensity (about 60 × 55 mm in its maximum extension), which could clearly be discriminated from surrounding brain tissue (Fig. 8.3c). Signal loss was visible on 15 slices in T2*-weighted images. Transplantation of 10,000 cells resulted in a circular but smaller area of signal extinction (about 3–4 mm in diameter, Fig. 8.3d), which was visible on 10 slices. A small but reproducible hypointensity with an average diameter of less than 2 mm was visible on 5 consecutive slices after transplantation of 1,000 VSOP-labeled MSC (Fig. 8.3e, white arrow head). However, transplantation of 500 cells did not lead to identical signal changes. A punctual hypointensity was found in the assumed area of the cell deposits in two out of three animals (Fig. 8.3f, white arrow head). In those two animals, subsequent histological analysis revealed microbleedings in the area of the cell deposit, which cannot be excluded as the origin of the signal extinctions. Microbleedings were not detected in the macroscopic tissue inspection (refer to Sect. 8.4 for details). Therefore, the in vivo detection limit of stereotaxically transplanted cells was defined at 1,000 cells at 3.0 T in T2*-weighted sequences in the healthy brain.

In the next step, we tested the hypothesis, whether VSOP-labeled MSC actively migrate toward an ischemic lesion. MSC were reported to mediate a multitude of beneficial effects following stroke and were shown to survive in the recipient brain for up to 1 year after intra-arterial administration (Shen et al. 2007a). Homing of MSC is presumed to be major element of the therapeutic effect by many investigators and was reported to depend on the SDF-1/CXCR4 system (Shichinohe et al. 2007). However, these mechanisms were only observed in rodent species; no evidence exists whether these effects can be reproduced in larger animals or human patients. This may be of critical relevance as, for instance, larger brain volumes and thereby longer traveling distances may hamper MSC homing toward and within the ischemic brain in large animal species and humans.

Transcranial permanent full cortical middle cerebral artery occlusion (MCAO) resulting in a large territorial infarct was induced in three Merino rams as described previously (Boltze et al. 2008). A brief description of the surgery is given in Fig. 8.4. The dose of administered VSOP-labeled cells was set to 1×10^6 per kilogram bodyweight. Cells were administered intravenously 24 ± 1 h after MCAO.

Sheep were subjected to 3.0 T MRI 24 h following MSC injection (48 h after MCAO) as well as 3 and 7 days thereafter. A short T2-weighted turbo spin echo

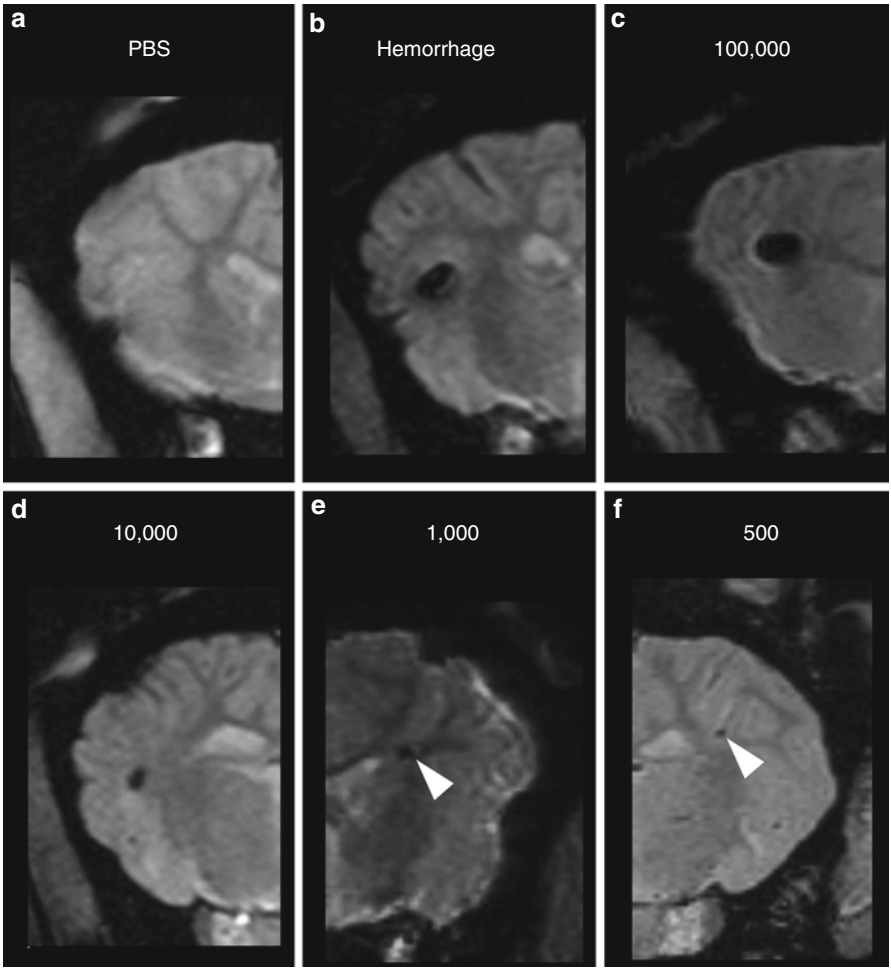

Fig. 8.3 Detection limit of VSOP-labeled autologous ovine MSC after stereotaxic cell administration at 3.0 T. Deposits containing a solution of VSOP-labeled, autologous MSC or PBS were injected stereotactically in the sheep brain (see Table 8.2). Brains were scanned using a T2* sequence (see Table 8.1). Injection of PBS did not result in any signal voids (**a**). A local hemorrhage, induced for control purposes, was visible as an irregular (ellipsoid-shaped) volume of signal loss (**b**), but was well discriminable from a cell deposit by histological investigation (see Sect. 8.2 and Fig. 8.4). 100,000 locally injected cells were clearly detectable at 3.0 T as a spherical signal extinction (**c**). The volume of the signal extinction became smaller after administration of 10,000 (**d**) or 1,000 cells (**e**, *white arrow head*). After injection of 500 cells, very small local signal extinction were seen at 3.0 T in 2 out of 3 subjects (**f**, *white arrow head*)

sequence (TSE, voxel size 0.55×0.55×2.5 mm, scanning time 6 min) was performed to visualize the stroke lesion (Fig. 8.5a), followed by a T2*-weighted sequence (see Table 8.1). A well discriminable and circumscribed hyperintense diffusion disturbance became evident in the supply area of the left middle cerebral

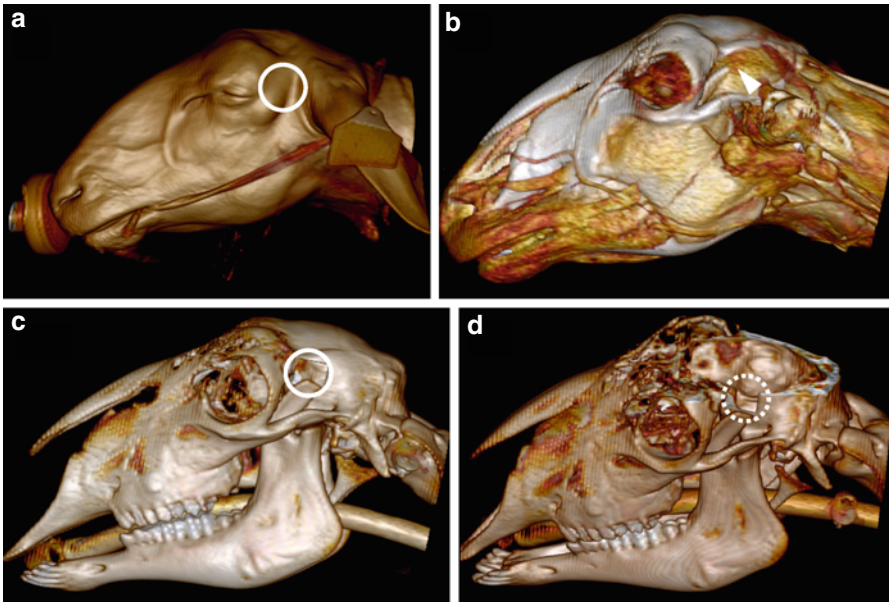

Fig. 8.4 Middle cerebral artery occlusion in sheep. Depicted, three-dimensional images of the sheep head and skull were reconstructed from a previously obtained computer tomography data set. Due to anatomical reason (paunch topography), the field of surgery must be on the left side of the head (**a**, *white circle*). After a skin incision, the temporal muscle (**b**, *white arrow head*) was elevated from the parietal skull bone. Subsequently, a craniotomy (**c**, *white circle*; **d**, *white dotted circle*) was performed using a high speed surgical burr. The middle cerebral artery was occluded by electrocauterization after local incision of the dura

artery in all subjects 2 days after MCAO (Fig. 8.5a). The area of ischemic damage mainly comprised the cortex and the white matter of the temporal lobe but also the claustrum and lateral areas of the external capsule as well as of the putamen. The lesion caused a clearly visible midline shift due to significant cytotoxic edema (Fig. 8.5b). It displaced normal radiological signs of reorganization and receding edema at day 3 (Fig. 8.5c) and day 7 (Fig. 8.5d) following MCAO. No further correlates for pathological events or processes could be observed in the TSE sequences. Furthermore, no hypointensities clearly attributable to VSOP-labeled MSC in the lesion or bordering areas in T2*-weighted imaging could be found (Fig. 8.5e–g) at any time point following MSC injection. Thus, there was no evidence for the homing of VSOP-labeled MSC after intravenous injection from MRI investigations.

8.4 Detection of VSOP-Labeled MSC *Ex Vivo*

Even though no signs for MSC homing toward the ischemic lesion were observed in MRI, minor numbers of migrated MSC below the detection threshold at 3.0 T may have been present in the brain. Moreover, labeled MSC may have migrated

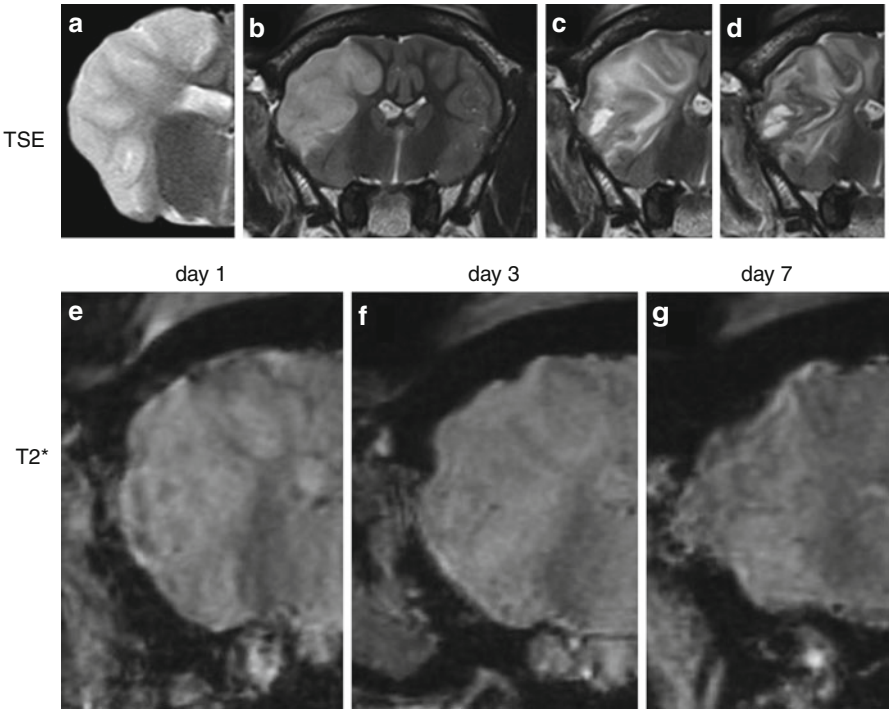

Fig. 8.5 MRI after intravenous injection of VSOP-labeled autologous MSC. A typical ischemic lesion (**a**) causing an obvious brain midline shift (**b**) was clearly detectable 2 days after middle cerebral artery occlusion in all subjects using a turbo spin echo (TSE) sequence. The lesion showed typical signs of reorganization 4 (**c**) and 8 (**d**) days after MCAO. Brain investigation using a T2* sequence according to Table 8.1 did not reveal any signal extinction caused by VSOP-labeled MSC 1 (**e**), 3 (**f**) or 7 (**g**) days after intravenous cell administration.

to other organs which were not investigated by MRI. A pathohistological tissue inspection (macroscopic and microscopic) was performed to reveal such potential events.

The induced hemorrhage induced in animal 1 of the local transplantation group was macroscopically visible (Fig. 8.6a, white dotted circle), whereas the site of PBS injection could not be identified. No signs for tissue damage or other (micro-) bleedings were observed on the macroscopic level after stereotaxic administration of the cells. The injection sites of 100,000 VSOP-labeled MSC could be identified as small brownish areas (Fig. 8.6b, black arrow head), which was not the case for 10,000 or less cells. For microscopic assessments, tissue samples were taken from the areas of stereotaxic injection or along the ischemic lesion, respectively. In MCAO subjects, corresponding tissue samples were also taken from the unaffected contralateral hemisphere and stained with hematoxylin/eosin (HE) or PB. Representative tissue samples were also taken from the sutured MCAO head wound (2× each), lung (4× each), liver, spleen, and kidneys.

All MSC deposits as well as the injection tracks could be identified histologically in serial slices from animals receiving stereotaxic cell transplantation. Locally transplanted, VSOP-labeled MSC could be identified as dense cell agglomerations in the HE stained white matter (Fig. 8.6c). Expectably, number and density of MSC became lower in deposits containing fewer cells. Mononuclear cells, which presumably immigrated to the injection site, were also found in and close to cell deposits. The presence of iron-containing cells was confirmed in PB staining (Fig. 8.6d). In some cases, scattered erythrocytes could be identified among the iron-labeled MSC. Erythrocytes could be clearly discriminated from iron-labeled MSC due to a much smaller size and their typical shape. However, in two out of three deposits containing 500 VSOP-labeled cells, a significant number of erythrocytes were visible next to PB-positive cells (Fig. 8.6e). Therefore, these events were considered microbleedings, which may have partially contributed to dot-like signal extinctions which were observed in MRI in these animals.

Histological investigation of the hemorrhage induced in animal 1 (control) revealed abundant erythrocytes and scattered mononuclear cells. The dimensions of this hemorrhage were comparable between MRI and tissue slices. In contrast, the signal extinction caused by labeled MSC was much larger as compared to the macroscopically visible cell deposit. This phenomenon is known as the blooming effect, being responsible for susceptibility artifacts that exceed the real dimension of an iron-labeled object by a factor of up to 50. The blooming effect, primarily emerging from the continuous biodegradation of hemoglobin into superparamagnetic hemosiderin, is less pronounced in early hemorrhages. Together with time-dependent changes of signal characteristics in hemorrhages (Kidwell and Wintermark 2008), this observation can help to discriminate signal extinctions caused by VSOP-labeled cells from those caused by hemorrhages.

Brain slices from animals that received intravenous administration of VSOP-labeled MSC were carefully examined to identify single PB cells at a 20-fold magnification. Only very few, scattered PB-positive cells (1–6 per slice) could be identified in the leptomeninx and the subarachnoid space (Fig. 8.7a, black arrow heads) of MCAO animals, but not in the brain parenchyma of the lesioned hemisphere (Fig. 8.7b). PB-positive cells could be observed neither in the contralateral leptomeninx (Fig. 8.7c) nor in the brain parenchyma of the contralateral hemisphere. Thus, no relevant homing of VSOP-labeled MSC toward the ischemic brain took place after systemic injection of the cells. PB-positive cells were also absent in the livers (Fig. 8.7d) and kidneys (Fig. 8.7e) of transplanted subjects. PB-positive cells could be indentified in the spleen of all animals (including control spleens from animals which were not subjected to MCAO or administration of VSOP-labeled cells, data not shown), presumably in the red pulp (Fig. 8.7f, white frame and insert). Scattered PB-positive cells were also observed in the white pulp, but only in animals which received MSC. Since the spleen is responsible for filtering and degradation of aged erythrocytes from the circulation, the presence of such cells in the spleen is not surprising. However, a large amount of PB-positive cells was identified in the lungs of all animals which received cell transplantation, but not in control tissue slices. These cells were distributed over the entire organ but mainly appeared in the alveoli

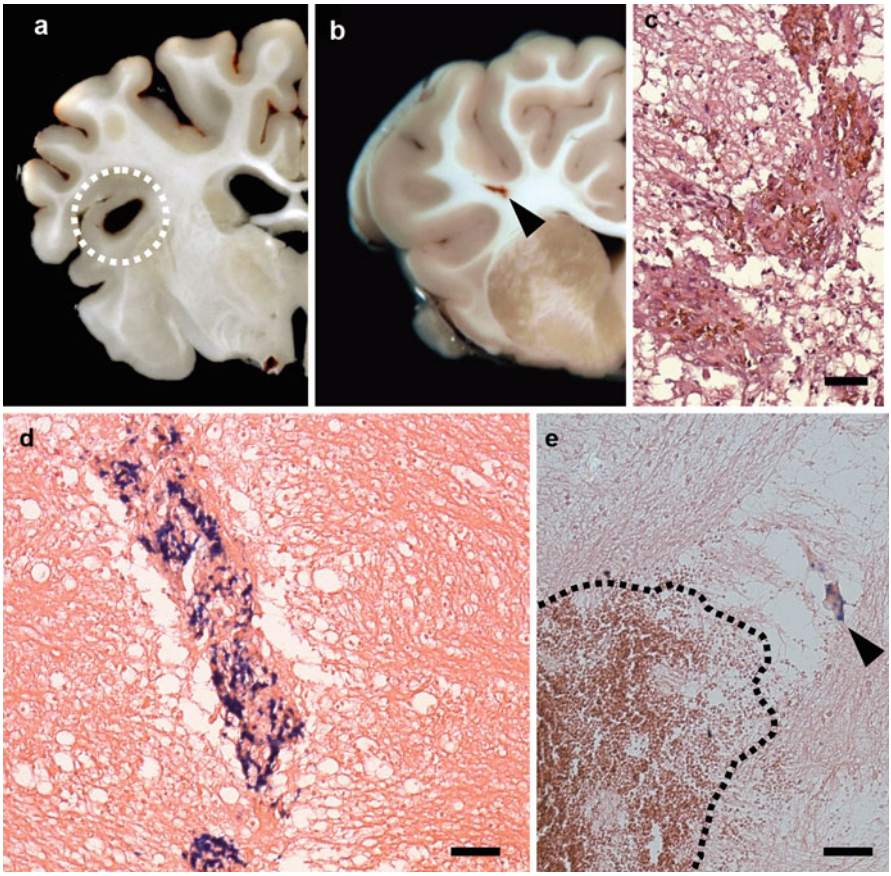

Fig. 8.6 Histological detection of stereotactically administered MSC. The sites of hemorrhage induction (**a**, *white dotted circle*) and the 100,000-cell deposit (**b**, *black arrow head*) were already visible in macroscopic brain slices. Local deposits of MSC were clearly detectable as dense structures in the HE (**c**). Prussian-blue staining (**d**) clearly revealed the presence of iron-containing cells at the site of local MSC deposits. However, in those animals in which signal extinction occurred after local administration of 500 cells, single Prussian-blue-positive cells (**e**, *black arrow head*) were observed in close proximity to small microbleedings in 2 of 3 cases (**e**, main part of microbleeding engulfed by *black dotted line*). Since this may have caused a unspecific signal loss, the in vivo detection limit was defined at 1,000 cells. Scale bars: 50 μm

and in the interstitial connective tissue (Fig. 8.7g), even though the cells could not be discriminated from pulmonary macrophages. This indicates a loss of VSOP-labeled MSC during pulmonary passages, but the amount of cell loss cannot be estimated from the obtained data. Interestingly, PB-positive cells which morphologically appeared similar to myofibroblasts were identified in areas of tissue restoration within the head wound (Fig. 8.7h). Similar cells were neither observed in skin samples from other areas in these animals nor in subjects which were not subjected to administration of VSOP-labeled MSC.

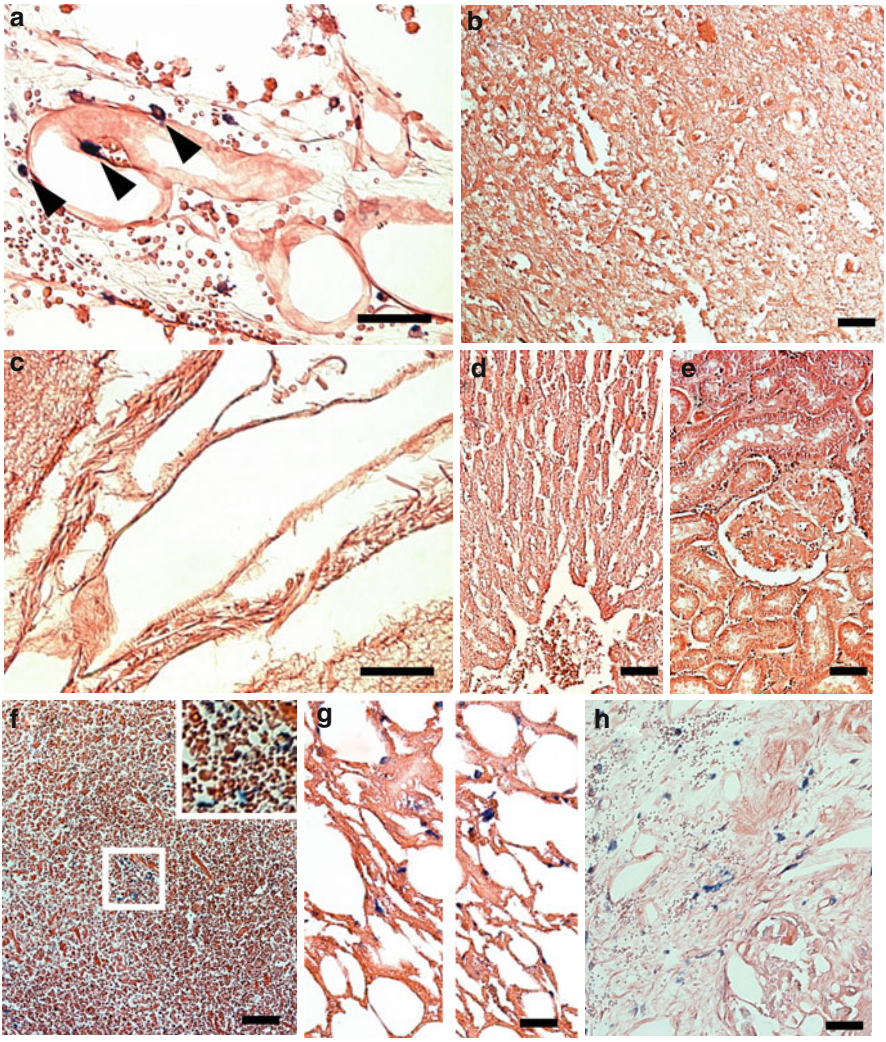

Fig. 8.7 Histological detection of intravenously injected MSC. No iron-containing cells were observed in the ipsilateral (lesioned) or contralateral gray or white matter. Very rarely, scattered Prussian-blue-positive cells were identified in the ipsilateral leptomeninx of MCAO animals (**a**, *black arrow heads*) but not in the ipsilateral brain parenchyma (**b**), the contralateral leptomenix (**c**), or the contralateral brain parenchyma. Further, no cells were observed in the liver (**d**) or kidneys (**e**) of transplanted subjects. Iron-containing, Prussian-blue-positive cells were found in the red pulp of the spleen in all subjects and control tissue samples from animals that did not receive VSOP-labeled MSC (**f**, high-power image of framed area given in *inset*). However, numerous MSC-like, iron containing cells were found in lungs (**g**) and the head wounds (**h**) of cell transplanted subjects. All images depict Prussian-blue stainings. Scale bars: 50 μm

Summarizing, there was no evidence for a target migration of magnetically labeled autologous MSC toward the ischemic lesion after systemic administration. In turn, some evidence was found that a significant proportion of cells got stuck in

the lungs whereas others potentially participated in wound healing processes. A final conclusion about the reasons of lacking cell migration would be preliminary because additional cell labeling techniques (e.g., using fluorescence dyes) or detailed description of the phenotype of PB-positive cells may be required to reveal conclusive information about cell fate.

Conclusions

The beneficial impact of systemically administered bone marrow-derived MSC after focal cerebral ischemia was reported in a number of studies. However, it still remains unclear whether these cells need to be located in areas bordering the ischemic tissue to induce these effects and whether a targeted homing of MSC is possible at all in large animals or humans, taken into account the substantially longer migration distances. To our knowledge, an experimental setup to investigate these questions using large animal models has not been developed up to now. The present study was designed to establish a labeling protocol for ovine MSC and to investigate the feasibility of autologous MSC tracking in sheep using a clinical MRI scanner. The study clearly revealed that ovine MSC can be detected both in gel phantoms and in vivo in the brain using a clinical 3.0 T MRI after VSOP labeling and autologous transplantation. Consequently, identification (and conceivably tracking) of labeled MSC by MRI in the sheep brain can be performed using a 3.0 T clinical scanner, without side effects of labeling procedure. Notably, our study revealed findings not reported in small animal models. The homing of bone marrow-derived MSC to the ischemic brain was repeatedly reported in rodent experiments (Chen et al. 2001; Wu et al. 2008). In contrast, in our experiments a significant migration toward infracted tissue was not observed.

Applying T2*-weighted sequences, the detection limit for MSC was found to be 500 cells in gel phantoms and 1,000 after local stereotaxic cell transplantation. Similar differences were also found in small animal models (Stroh et al. 2005) and are at least in part attributable to the compromise between image quality on the one side and demands of imaging setup in animals (particularly scan time but also available coils as well as scanner hard- and software configuration) on the other. Thus, alternative imaging sequences allowing for faster scan performance at same or even higher sensitivity for susceptibility differences or changes as compared to T2*-weighted sequences may be demanded. Moreover, sequences particularly prone to field inhomogeneities such as T2*-weighted sequences may require custom-built coils and elaborated nonlinear shimming, still limiting cell detection in common T2* sequences (Pillai et al. 2011; Denic et al. 2011).

Susceptibility-weighted imaging (SWI) is characterized by a very high sensitivity for magnetic field distortions caused by paramagnetic and ferromagnetic substances, leading to negative contrast signal voids. The sensitivity of SWI sequences is discussed to be significantly higher compared to T2*-based imaging (Sehgal et al. 2005; Dai et al. 2011), but discrimination between hemorrhages and VSOP-induced signal changes remains difficult with SWI sequences (Haacke et al. 2009). Nevertheless, an assessment of the applicability of SWI for MSC tracking in the large animal brain including a direct comparison to a T2*-weighted sequence should be performed in future experiments, particularly for

the detection of comparatively small numbers of labeled cells that migrated to the lesion site and may only be detectable with an optimized imaging setup. However, MSC could be identified using T2*-weighted MRI after local injection also in relatively small numbers of 1,000 MSC in a deposit. Moreover, no indications for the presence of iron-loaded cells in brain parenchyma were observed after systemic administration. Insufficient field strength and/or sequence parameters being unable to detect minor cell numbers are therefore rendered unlikely to be the sole reason for lacking cell detection by MRI. More likely, there was only a very limited or even no migration of autologous MSC to the ovine brain.

The number of cells injected in this study was 1×10^6 per kg bodyweight. Usually, between 1×10^6 (e.g., Chen et al. 2003) and 3×10^6 (e.g., Okazaki et al. 2008) are reported to be administered in a rat, with 3×10^6 cells being reported effective (Chen et al. 2001). The average weight of adult laboratory is strain-dependent but can be found in the range of 300–450 g. Thus, the number of cells injected into sheep is relatively small, but a histologically detectable number of MSC should have reached the brain parenchyma also after administration of a "subtherapeutic" MSC dose. Moreover, iron-containing cells were detected in other tissues including the leptomeninx so an insufficient cell number for administration is unlikely the cause for unsuccessful detection of cell homing to the ischemic lesion (Sect. 3). The SDF-1/CXCR4 system, which is reported to mediate MSC migration to an ischemic lesion (Shichinohe et al. 2007), is also relevant for attracting immune cells during the inflammatory as well as the proliferative phase of wound healing processes in numerous tissues including the skin (Shichinohe et al. 2007; Ding et al. 2011; Hannoush et al. 2011; Fujio et al. 2011). In fact, iron-containing cells were identified in the skin wounds of animals of MSC-treated subjects. These cells were observed in skin wound samples from animals which did not receive VSOP-labeled cells. This indicates that a targeted homing of MSC to a side of injury is in principle possible. It may also be hypothesized that the migratory stimulus emerging from the head wound may competitively interact with the one resulting from the ischemic brain lesion.

Numerous iron-loaded cells have been found in the ovine lungs after intravenous cell administration. The identity of these cells is hard to unambiguously assess in an autologous setup, but similar cells were not found in untreated subjects. It may be assumed that these cells are in fact injected MSC since immunologic rejection or destruction of autologous MSC, even after *ex vivo* processing, has not been reported so far. Moreover, a "filter effect" of the lungs for MSC, but not for mononuclear cells, was reported in a rodent study (Fischer et al. 2009). This is reasonable considering the fact that MSC (1,000–7,000 μm^3) are significantly larger than MNC (100–350 μm^3). Further assuming MSC being spheroid entities when traveling in the blood stream, the cells would have a diameter between 12.4 and 23.7 μm. This is by far larger than the average diameter of pulmonary capillaries (5–10 μm), which may contribute to the filter effect even though MSC cannot be considered "rigid" cells.

Given the reported benefit of MSC administration after stroke, additional strategies will most likely be required to enhance the number of MSC homing to the cerebral lesion in order to improve the therapeutic impact. The impact of this

alternative administration rout needs to be investigated in this particular model. For example, intra-arterial cell delivery may help to reduce the amount of MSC filtered from the lungs, at least during the first passage after cell injection. Additionally, the influence of strategies aiming to enhancing migration capabilities of MSC to lesioned areas by cell surface engineering (Sarkar et al. 2011a, b) will have to be assessed in further studies.

References

Arbab AS, Bashaw LA, Miller BR, Jordan EK, Bulte JW, Frank JA (2003) Intracytoplasmic tagging of cells with ferumoxides and transfection agent for cellular magnetic resonance imaging after cell transplantation: methods and techniques. Transplantation 76:1123–1130

Bang OY, Lee JS, Lee PH, Lee G (2005) Autologous mesenchymal stem cell transplantation in stroke patients. Ann Neurol 57:874–882

Bao X, Feng M, Wei J, Han Q, Zhao H, Li G, Zhu Z, Xing H, An Y, Qin C, Zhao RC, Wang R (2011) Transplantation of Flk-1+ human bone marrow-derived mesenchymal stem cells promotes angiogenesis and neurogenesis after cerebral ischemia in rats. Eur J Neurosci 34:87–98

Barbosa da Fonseca LM, Gutfilen B, Rosado de Castro PH, Battistella V, Goldenberg RC, Kasai-Brunswick T, Chagas CL, Wajnberg E, Maiolino A, Salles XS, Andre C, Mendez-Otero R, de Freitas GR (2010) Migration and homing of bone-marrow mononuclear cells in chronic ischemic stroke after intra-arterial injection. Exp Neurol 221:122–128

Boltze J, Forschler A, Nitzsche B, Waldmin D, Hoffmann A, Boltze CM, Dreyer AY, Goldammer A, Reischauer A, Hartig W, Geiger KD, Barthel H, Emmrich F, Gille U (2008) Permanent middle cerebral artery occlusion in sheep: a novel large animal model of focal cerebral ischemia. J Cereb Blood Flow Metab 28:1951–1964

Bonita R, Mendis S, Truelsen T, Bogousslavsky J, Toole J, Yatsu F (2004) The global stroke initiative. Lancet Neurol 3:391–393

Burns TC, Steinberg GK (2011) Stem cells and stroke: opportunities, challenges and strategies. Expert Opin Biol Ther 11:447–461

Chen J, Li Y, Wang L, Zhang Z, Lu D, Lu M, Chopp M (2001) Therapeutic benefit of intravenous administration of bone marrow stromal cells after cerebral ischemia in rats. Stroke 32:1005–1011

Chen J, Zhang ZG, Li Y, Wang L, Xu YX, Gautam SC, Lu M, Zhu Z, Chopp M (2003) Intravenous administration of human bone marrow stromal cells induces angiogenesis in the ischemic boundary zone after stroke in rats. Circ Res 92:692–699

Daadi MM, Li Z, Arac A, Grueter BA, Sofilos M, Malenka RC, Wu JC, Steinberg GK (2009) Molecular and magnetic resonance imaging of human embryonic stem cell-derived neural stem cell grafts in ischemic rat brain. Mol Ther 17:1282–1291

Dai Y, Zeng M, Li R, Rao S, Chen C, DelProposto Z, Haacke EM, Hu J, Renate J (2011) Improving detection of siderotic nodules in cirrhotic liver with a multi-breath-hold susceptibility-weighted imaging technique. J Magn Reson Imaging 34:318–325

de Vries IJ, Lesterhuis WJ, Barentsz JO, Verdijk P, van Krieken JH, Boerman OC, Oyen WJ, Bonenkamp JJ, Boezeman JB, Adema GJ, Bulte JW, Scheenen TW, Punt CJ, Heerschap A, Figdor CG (2005) Magnetic resonance tracking of dendritic cells in melanoma patients for monitoring of cellular therapy. Nat Biotechnol 23:1407–1413

Denic A, Macura SI, Mishra P, Gamez JD, Rodriguez M, Pirko I (2011) MRI in rodent models of brain disorders. Neurotherapeutics 8:3–18

Ding J, Hori K, Zhang R, Marcoux Y, Honardoust D, Shankowsky HA, Tredget EE (2011) Stromal cell-derived factor 1 (SDF-1) and its receptor CXCR4 in the formation of postburn hypertrophic scar (HTS). Wound Repair Regen 19:568–578

Dreyer A, Stroh A, Pösel C, Findeisen M, von Geymüller T, Lobsien D, Nitzsche B, Boltze J (2012) Frameless stereotaxy in sheep – neurosurgical and imaging techniques for transla-

tional stroke research. In: Balestrino M (ed) Advances in the preclinical study of ischemic stroke, 1st edn. InTech, Rijeka
Emre U, Rantanen K, Tatlisumak T (2007) Antithrombotic treatment in the prevention of ischemic stroke. Curr Drug Targets 8:817–823
Falluji N, Abou-Chebl A, Rodriguez Castro CE, Mukherjee D (2012) Reperfusion strategies for acute ischemic stroke. Angiology 63:289–296
Fischer UM, Harting MT, Jimenez F, Monzon-Posadas WO, Xue H, Savitz SI, Laine GA, Cox CS Jr (2009) Pulmonary passage is a major obstacle for intravenous stem cell delivery: the pulmonary first-pass effect. Stem Cells Dev 18:683–692
Frey S, Comeau R, Hynes B, Mackey S, Petrides M (2004) Frameless stereotaxy in the nonhuman primate. Neuroimage 23:1226–1234
Fujio M, Yamamoto A, Ando Y, Shohara R, Kinoshita K, Kaneko T, Hibi H, Ueda M (2011) Stromal cell-derived factor-1 enhances distraction osteogenesis-mediated skeletal tissue regeneration through the recruitment of endothelial precursors. Bone 49:693–700
Haacke EM, Mittal S, Wu Z, Neelavalli J, Cheng YC (2009) Susceptibility-weighted imaging: technical aspects and clinical applications, part 1. AJNR Am J Neuroradiol 30:19–30
Hannoush EJ, Sifri ZC, Elhassan IO, Mohr AM, Alzate WD, Offin M, Livingston DH (2011) Impact of enhanced mobilization of bone marrow derived cells to site of injury. J Trauma 71:283–289
Honmou O, Houkin K, Matsunaga T, Niitsu Y, Ishiai S, Onodera R, Waxman SG, Kocsis JD (2011) Intravenous administration of auto serum-expanded autologous mesenchymal stem cells in stroke. Brain 134:1790–1807
Jang KS, Lee KS, Yang SH, Jeun SS (2010) In vivo tracking of transplanted bone marrow-derived mesenchymal stem cells in a murine model of stroke by bioluminescence imaging. J Korean Neurosurg Soc 48:391–398
Jensen MB, Yan H, Krishnaney-Davison R, Al SA, Zhang SC (2011) Survival and differentiation of transplanted neural stem cells derived from human induced pluripotent stem cells in a rat stroke model. J Stroke Cerebrovasc Dis. PMID: 22078778
Kidwell CS, Wintermark M (2008) Imaging of intracranial haemorrhage. Lancet Neurol 7:256–267
Kim D, Chun BG, Kim YK, Lee YH, Park CS, Jeon I, Cheong C, Hwang TS, Chung H, Gwag BJ, Hong KS, Song J (2008) In vivo tracking of human mesenchymal stem cells in experimental stroke. Cell Transplant 16:1007–1012
Kranz A, Wagner DC, Kamprad M, Scholz M, Schmidt UR, Nitzsche F, Aberman Z, Emmrich F, Riegelsberger UM, Boltze J (2010) Transplantation of placenta-derived mesenchymal stromal cells upon experimental stroke in rats. Brain Res 1315:128–136
Langhorne P, Bernhardt J, Kwakkel G (2011) Stroke rehabilitation. Lancet 377:1693–1702
Lansberg MG, Bluhmki E, Thijs VN (2009) Efficacy and safety of tissue plasminogen activator 3 to 4.5 hours after acute ischemic stroke: a metaanalysis. Stroke 40:2438–2441
Lin YC, Ko TL, Shih YH, Lin MY, Fu TW, Hsiao HS, Hsu JY, Fu YS (2011) Human umbilical mesenchymal stem cells promote recovery after ischemic stroke. Stroke 42:2045–2053
Minnerup J, Kim JB, Schmidt A, Diederich K, Bauer H, Schilling M, Strecker JK, Ringelstein EB, Sommer C, Scholer HR, Schabitz WR (2011) Effects of neural progenitor cells on sensorimotor recovery and endogenous repair mechanisms after photothrombotic stroke. Stroke 42:1757–1763
Muja N, Bulte JW (2009) Magnetic resonance imaging of cells in experimental disease models. Prog Nucl Magn Reson Spectrosc 55:61–77
Nagai N, Kawao N, Okada K, Okumoto K, Teramura T, Ueshima S, Umemura K, Matsuo O (2010) Systemic transplantation of embryonic stem cells accelerates brain lesion decrease and angiogenesis. Neuroreport 21:575–579
Natarajan SK, Snyder KV, Siddiqui AH, Ionita CC, Hopkins LN, Levy EI (2009) Safety and effectiveness of endovascular therapy after 8 hours of acute ischemic stroke onset and wake-up strokes. Stroke 40:3269–3274
Okazaki T, Magaki T, Takeda M, Kajiwara Y, Hanaya R, Sugiyama K, Arita K, Nishimura M, Kato Y, Kurisu K (2008) Intravenous administration of bone marrow stromal cells increases survivin and Bcl-2 protein expression and improves sensorimotor function following ischemia in rats. Neurosci Lett 430:109–114

Pillai DR, Heidemann RM, Kumar P, Shanbhag N, Lanz T, Dittmar MS, Sandner B, Beier CP, Weidner N, Greenlee MW, Schuierer G, Bogdahn U, Schlachetzki F (2011) Comprehensive small animal imaging strategies on a clinical 3 T dedicated head MR-scanner; adapted methods and sequence protocols in CNS pathologies. PLoS One 6:e16091

Pittenger MF (2008) Mesenchymal stem cells from adult bone marrow. Methods Mol Biol 449:27–44

Sarkar D, Spencer JA, Phillips JA, Zhao W, Schafer S, Spelke DP, Mortensen LJ, Ruiz JP, Vemula PK, Sridharan R, Kumar S, Karnik R, Lin CP, Karp JM (2011a) Engineered cell homing. Blood 118:e184–e191

Sarkar D, Zhao W, Gupta A, Loh WL, Karnik R, Karp JM (2011b) Cell surface engineering of mesenchymal stem cells. Methods Mol Biol 698:505–523

Savitz SI, Chopp M, Deans R, Carmichael ST, Phinney D, Wechsler L (2011) Stem cell therapy as an emerging paradigm for stroke (STEPS) II. Stroke 42:825–829

Sehgal V, DelProposto Z, Haacke EM, Tong KA, Wycliffe N, Kido DK, Xu Y, Neelavalli J, Haddar D, Reichenbach JR (2005) Clinical applications of neuroimaging with susceptibility-weighted imaging. J Magn Reson Imaging 22:439–450

Seminatore C, Polentes J, Ellman D, Kozubenko N, Itier V, Tine S, Tritschler L, Brenot M, Guidou E, Blondeau J, Lhuillier M, Bugi A, Aubry L, Jendelova P, Sykova E, Perrier AL, Finsen B, Onteniente B (2010) The postischemic environment differentially impacts teratoma or tumor formation after transplantation of human embryonic stem cell-derived neural progenitors. Stroke 41:153–159

Shen LH, Li Y, Chen J, Cui Y, Zhang C, Kapke A, Lu M, Savant-Bhonsale S, Chopp M (2007a) One-year follow-up after bone marrow stromal cell treatment in middle-aged female rats with stroke. Stroke 38:2150–2156

Shen LH, Li Y, Chen J, Zacharek A, Gao Q, Kapke A, Lu M, Raginski K, Vanguri P, Smith A, Chopp M (2007b) Therapeutic benefit of bone marrow stromal cells administered 1 month after stroke. J Cereb Blood Flow Metab 27:6–13

Shen LH, Li Y, Gao Q, Savant-Bhonsale S, Chopp M (2008) Down-regulation of neurocan expression in reactive astrocytes promotes axonal regeneration and facilitates the neurorestorative effects of bone marrow stromal cells in the ischemic rat brain. Glia 56:1747–1754

Shichinohe H, Kuroda S, Yano S, Hida K, Iwasaki Y (2007) Role of SDF-1/CXCR4 system in survival and migration of bone marrow stromal cells after transplantation into mice cerebral infarct. Brain Res 1183:138–147

Shobha N, Buchan AM, Hill MD (2011) Thrombolysis at 3–4.5 hours after acute ischemic stroke onset–evidence from the Canadian Alteplase for Stroke Effectiveness Study (CASES) registry. Cerebrovasc Dis 31:223–228

Stroh A, Zimmer C, Gutzeit C, Jakstadt M, Marschinke F, Jung T, Pilgrimm H, Grune T (2004) Iron oxide particles for molecular magnetic resonance imaging cause transient oxidative stress in rat macrophages. Free Radic Biol Med 36:976–984

Stroh A, Faber C, Neuberger T, Lorenz P, Sieland K, Jakob PM, Webb A, Pilgrimm H, Schober R, Pohl EE, Zimmer C (2005) In vivo detection limits of magnetically labeled embryonic stem cells in the rat brain using high-field (17.6 T) magnetic resonance imaging. Neuroimage 24:635–645

Stroh A, Zimmer C, Werner N, Gertz K, Weir K, Kronenberg G, Steinbrink J, Mueller S, Sieland K, Dirnagl U, Nickenig G, Endres M (2006) Tracking of systemically administered mononuclear cells in the ischemic brain by high-field magnetic resonance imaging. Neuroimage 33:886–897

Stroh A, Boltze J, Sieland K, Hild K, Gutzeit C, Jung T, Kressel J, Hau S, Reich D, Grune T, Zimmer C (2009) Impact of magnetic labeling on human and mouse stem cells and their long-term magnetic resonance tracking in a rat model of Parkinson disease. Mol Imaging 8:166–178

Tsai LK, Wang Z, Munasinghe J, Leng Y, Leeds P, Chuang DM (2011) Mesenchymal stem cells primed with valproate and lithium robustly migrate to infarcted regions and facilitate recovery in a stroke model. Stroke 42:2932–2939

Ukai R, Honmou O, Harada K, Houkin K, Hamada H, Kocsis JD (2007) Mesenchymal stem cells derived from peripheral blood protects against ischemia. J Neurotrauma 24:508–520

Vahedi K, Hofmeijer J, Juettler E, Vicaut E, George B, Algra A, Amelink GJ, Schmiedeck P, Schwab S, Rothwell PM, Bousser MG, van der Worp HB, Hacke W (2007) Early decompressive surgery in malignant infarction of the middle cerebral artery: a pooled analysis of three randomised controlled trials. Lancet Neurol 6:215–222

Wu J, Sun Z, Sun HS, Wu J, Weisel RD, Keating A, Li ZH, Feng ZP, Li RK (2008) Intravenously administered bone marrow cells migrate to damaged brain tissue and improve neural function in ischemic rats. Cell Transplant 16:993–1005